

Thickness driven stabilization of saw-tooth like domains upon phase transitions in ferroelectric thin films with depletion charges

I. B. Misirlioglu*, H. N. Cologlu, M. Yildiz

Faculty of Engineering and Natural Sciences, Sabanci University, Tuzla/Orhanli, 34956

Istanbul, Turkey

Abstract

Ionized impurities have nearly always been neglected in discussing the limit of functionality of ferroelectric thin films. One would certainly expect that the thickness limit for functionality would be altered in the presence of ionized impurities but how this would occur remains unclear. In this article, we analyze the domain structures as well as the phase transition temperatures in films with depletion charges for various film thicknesses. Due to the inhomogeneity created by depletion charges, saw-tooth like domain structures develop spanning the entire film thickness that are possible in films with depletion charges having perfect electrode screening, i. e., ideal electrodes if the film is above a critical thickness. On the other hand, the phase transition of the ultrathin structures with dead layers is always into the multidomain state during cooling from the paraelectric state regardless of the presence of depletion charges. Transition temperature in films with dead layers does not depend nearly at all on the depletion charge density unless it is very high ($>10^{26}$ ionized impurities/m³). Relatively thick films (>8 nm in this work) with dead layers that have very high depletion charge densities have transition temperatures very similar to those with the same charge density but with ideal electrodes, making us conclude that thick films with high depletion charge densities will hardly feel the dead layer effects. The results are provided for (001) BaTiO₃ films grown on (001) SrTiO₃ substrates with pseudomorphic top and bottom metallic electrodes.

Keywords: Ferroelectric films, depletion charge, electrostatics, phase transition, thermodynamic simulation.

*Author to whom correspondance should be addressed: burc@sabanciuniv.edu

1. Introduction

The intrinsic limit of ferroelectricity in thin films has been a topic of extensive discussions in many reports. A strained, planarly confined thin ferroelectric (FE) structure exhibits dramatic changes in the dipole configurations commensurate with strong deviations from bulk states. One fact is that the formation of defects such as ionic vacancies, interstitials and dislocation networks are inevitable owing to both the process conditions and the developing strains in the film on misfitting substrates during fabrication. The defect fields and their impact on the physical properties of FEs both in bulk and film form have been the focus of numerous studies including dedicated book chapters [1-14]. It has been well understood that the vacancy or impurity type point defects lead to a depletion zone upon formation of the metal-film contact during electroding. The motivation to study such material systems has been to understand the limit of existence of ferroelectricity as a function of thickness and electrode-interface conditions, particularly focusing on depolarizing field effects [15-25]. A recent study, for example, based on a first principles approach reports that a possible asymmetry in the material type for the top-bottom film-electrode contacts could compete with the depolarizing effects through an internal bias field and reduce the critical thickness of a switchable ferroelectric polarization's existence to about two unit cells [26]. Besides applications in nano scale memory devices, field effect transistors and tunable layers in integrated circuits [4, 24, 27], these materials have also become a test-bed in the past few decades for studying phase transitions and critical behavior in the solid state probably only second to magnetic materials.

Fabrication of these systems in capacitor geometries naturally results in the equilibration of the chemical potential at the metal-ferroelectric interfaces in ferroelectric films that often have impurity states and the formation of a charged region on the film side is nearly inevitable. This has been mostly analyzed experimentally in addition to a few theoretical studies [11, 29-31] including attempts in artificially graded structures [32]. As will be shown, the depletion charge itself acts as a source of inhomogeneity and the situation is not very different from introducing compositional gradients to the system. Recently, several works have been devoted to especially understand the evolution of these charges under limited lattice diffusivities but how such phenomena will be impacted by size effects remain an important aspect to be understood [33, 34]. Furthermore, it is well known that charged defects such as impurities and vacancies will be quite immobile at temperatures near room temperature (RT) and might get populated at interfaces and defect sites probably only after several thousands of applied field cycles [7, 35].

In a real ultrathin ferroelectric film, due to the very short distances at which potential drops occur, it becomes very crucial to elaborate the interaction between depletion charges and the consequences of the extent of screening at the film-electrode interface. As the film thickness, when at the order of a few tens of nm or less, can be comparable or smaller than the depletion zone width in a ferroelectric in contact with electrodes that has typical densities of impurities, the entire ultrathin film can be said to be depleted and that the ionized impurities are nearly homogeneously distributed. Depletion widths of around 30 nm and ionized impurity densities of around $10^{25-27}/\text{m}^3$ has

been reported by Pintilie *et al.* using interfacial capacitance measurements for $\text{PbZr}_{0.2}\text{Ti}_{0.8}\text{O}_3$ films [35, 36].

The attempts to clarify the depletion charge effects have mostly been confined to very simple charge distributions as analysis of realistic distributions, even when depletion charge density is homogeneous, via analytical approaches can become a formidable problem. Only a few studies exist that try to analyze the effects of continuous depletion charge distributions on the observable properties in relatively thick films [7, 38-40] but these studies have considered the single domain states. The possibility that, due to the inhomogeneous nature of the system owing to depletion charges, the transition could be into multidomain states even in structures with ideal electrodes would make a prominent difference in the calculated transition temperatures, which is one of the main emphasis given in this paper. The way in which phase transition characteristics would be altered is discussed rigorously by Bratkovsky and Levanyuk [29] in the absence of dead layers. Reduction in the critical temperature commensurate with smaller coercivities in the ferroelectric state was demonstrated along with a qualitative discussion on the possibility of domain formation. One could easily foresee that the conclusions withdrawn for systems with ideal electrodes will have to be modified, for instance, for systems that have imperfect film-electrode interfaces, namely real electrodes. This latter statement is indeed a very important one when discussing experimental results on ferroelectric stability in the light of electrostatic considerations.

In this article, we address the question as to whether or not depletion charge effects could compete and overwhelm dead layer effects due to conditions at the film-electrode interfaces. To probe the competing energies, we use the Landau-Ginzburg-

Devonshire (LGD) formalism for ferroelectric materials coupled with the interface conditions and presence of depletion charges. Firstly, films of various thickness with perfect film-electrode interfaces, namely ideal electrodes, but with depletion charges are analyzed. A saw-tooth type domain structure forms in relatively thick films due to the inhomogeneous internal field. At the transition temperature, thick films with ideal electrodes but high depletion charge density always exhibit the saw-tooth domains. The period of this domain structure grows with increasing film thickness. Following this analysis, we introduce thin dead layers at the film-electrode interfaces to find out the possible alterations to the domain configurations and sensitivity of the domains to thickness effects. We found out that the domain period in a film having dead layers are altered upon introduction of a homogeneous depletion charge density to the system. At high depletion charge densities, domains with a saw-tooth type structure regardless of the presence of the dead layers. We also show that the transition temperatures are significantly lowered in relatively thick films with high depletion charge densities and dead layers while this lowering is minimal in the thinner films and remain nearly unchanged with respect to charge-free films with dead layers. This behavior is a direct consequence of the dead layer effects dominating at low thicknesses while thicker films are under a heavier influence of depletion charges. Our results reveal the magnitudes of changes that can be expected in the transition temperatures for films with depletion charges considering especially the transition into multidomain states.

2. Theory and Methodology

In this section we give the governing equations and boundary conditions used to obtain field and temperature dependent characteristics of the ferroelectric thin film capacitors. The schematics of the geometries considered is given in Figure 1. A two dimensional grid is constructed that has $200n \times kn$ cells where k (200) is the number of cells along the film thickness (width) and each cell, n , has a dimension of 0.4 nm, nearly the lattice parameters of well known pseudocubic perovskites such as BT to imitate the order of lengths at which P can vary in the system compared to real systems. Polarization is obtained by solving the equations of state derived from the LGD free energy for all P in our system for an epitaxial monodomain (001) BaTiO₃ ferroelectric film on a (001) SrTiO₃ cubic substrate along with the Maxwell equation for dielectric displacement employing a finite difference discretization. The strain states of the films determine the stable P components. We partition the thin film capacitor system along the thickness axis, z , as follows:

$$\begin{aligned} w=1 & \text{ when } -h/2 \leq z \leq +h/2 \\ w=0 & \text{ when } -h/2-d < z < -h/2 \text{ and } +h/2 < z < d+h/2, \end{aligned} \quad (1)$$

where w is a step-wise function defining the interface between the dead layer and the ferroelectric and d is the dead layer thickness (taken as 1 unit cell thick, ~ 0.4 nm in this work), $|h|$ is the thickness of the ferroelectric layer. The electrode-dead layer interfaces are at $-h/2-d$ and $d+h/2$ respectively. Note that $d = 0$ indicates the absence of a dead layer, i. e., a perfect film-electrode contact interface. The equations of state for the system

to define the relation between the fields in the layers and the P components as well as $\boldsymbol{\varepsilon}_r$ of the dead layers using the definition of w in Eqn. 1 are,

$$\begin{aligned}
& w(2\alpha_3^m P_3 + 4\alpha_{13}^m P_3 P_1^2 + 4\alpha_{33}^m P_3^3 + 6\alpha_{111} P_3^5 \\
& + \alpha_{112} (4P_3 P_1^4 + 8P_3^3 P_1^2) + 2\alpha_{123} P_3 P_1^4 - G_{33} \frac{d^2 P_3}{dz^2} - G_{13} \frac{d^2 P_3}{dx^2}) + (1-w) \frac{D_3}{\boldsymbol{\varepsilon}_r \boldsymbol{\varepsilon}_0} \\
& = wE_3^F + (1-w)E_3^d
\end{aligned} \tag{2a}$$

$$\begin{aligned}
& w(2\alpha_1^m P_1 + 2(2\alpha_{11}^m + \alpha_{12}^m)P_1^3 + 2\alpha_{13}^m P_1 P_3^2 + 6\alpha_{111} P_1^5 + \\
& 2\alpha_{112} [3P_1^5 + 3P_1^3 P_3^2 + P_1 P_3^4] + 2\alpha_{123} P_1^3 P_3^2 - G_{31} \frac{d^2 P_1}{dz^2} + G_{11} \frac{d^2 P_1}{dx^2}) + (1-w) \frac{D_1}{\boldsymbol{\varepsilon}_r \boldsymbol{\varepsilon}_0} \\
& = wE_1^F + (1-w)E_1^d
\end{aligned} \tag{2b}$$

where P_i ($i=1,2,3$) are the components of P in the ferroelectric state, α_3^m , α_{13}^m , α_{33}^m , α_1^m , α_{11}^m , α_{12}^m are the renormalized dielectric stiffness coefficients, modified by the misfit strain and the two-dimensional clamping of the film, while α_{111} , α_{112} , α_{123} are the dielectric stiffness coefficients in the bulk [41], G_{ij} are the gradient energy coefficients. For the sake of convenience, we shall assume that the gradient energy coefficient is isotropic, and thus $G_{33} = G_{31} = G_{13} = G_{11} = G_{23} = G_{21} = G$. $G = 3 \times 10^{-10}$ and is proportional to $\delta^2 (T_C / \boldsymbol{\varepsilon}_0 C)$ with δ being a distance at the order of a unit-cell, T_C the Curie point, $\boldsymbol{\varepsilon}_0$ the permittivity of free space and C the Curie constant. We also neglect the gradients in P_2 along y within the two dimensional limit. E_3^F, E_1^F and E_3^d, E_1^d are the fields along z - and x -axis in the ferroelectric layer and the dead layer respectively. The equality between the field and the dielectric displacement in the dead layer ($w=0$) reads

$$\mathbf{D}_3 = \epsilon_r \epsilon_0 \mathbf{E}_3^d \text{ and } \mathbf{D}_1 = \epsilon_r \epsilon_0 \mathbf{E}_1^d \quad (3)$$

and for $w=1$ (ferroelectric layer),

$$\mathbf{D}_3 = \epsilon_b \epsilon_0 \mathbf{E}_3^F + \mathbf{P}_3 \text{ and } \mathbf{D}_1 = \epsilon_b \epsilon_0 \mathbf{E}_1^F + \mathbf{P}_1 \quad (4)$$

The dead layer, when present, is assumed to be a high- k dielectric whose dielectric constant, ϵ_r , is 20 to exemplify its effects and ϵ_b is the background dielectric constant of the ferroelectric (taken as 7 in this work). The electric fields in both the ferroelectric layer and the dead layer are computed from the gradients of the electrostatic potential from

$$\mathbf{E}_3^F = -\frac{d\phi^F}{dz}, \quad \mathbf{E}_1^F = -\frac{d\phi^F}{dx} \quad (5)$$

for the ferroelectric and

$$\mathbf{E}_3^d = -\frac{d\phi^d}{dz}, \quad \mathbf{E}_1^d = -\frac{d\phi^d}{dx} \quad (6)$$

in the dead layers with ϕ^F and ϕ^d being the electrostatic potential in the ferroelectric and the dead layer respectively. The electrostatic potential in each layer can be found at each point as function of P and the dielectric constant of the dead layer using the Maxwell relation in the absence of free charges $\nabla \cdot \mathbf{D} = 0$ and $\nabla \cdot \mathbf{D} = \rho$ when depletion charges due to ionized impurities are present. ρ is the volumetric charge density (0 when no impurities are present). Thus one has

$$\frac{d^2 \phi^F}{dz^2} + \frac{d^2 \phi^F}{dx^2} = \frac{1}{\epsilon_b \epsilon_0} \left(\frac{dP_3}{dz} + \frac{dP_1}{dx} - \rho \right) \quad (7)$$

in the ferroelectric layer and

$$\frac{d^2 \phi^d}{dz^2} + \frac{d^2 \phi^d}{dx^2} = \frac{\rho}{\epsilon_r \epsilon_0} \quad (8)$$

for the dead layer. We assume that each impurity contributing to ρ has only one positive unit charge (the charge of one electron) in all cases. The depletion charge density in this work is assumed to be constant throughout the film volume, which is indeed realistic enough for thicknesses at the order of a few tens of nanometers (See Refs. 30, 36-37). The boundary conditions we employed for $P_{1,3}$ are

$$\left[P_1 + \lambda \frac{dP_1}{dz} \right]_{z=-\frac{h}{2}-d, \frac{h}{2}+d} = 0, \left[P_3 + \lambda \frac{dP_3}{dz} \right]_{z=-\frac{h}{2}-d, \frac{h}{2}+d} = 0 \quad (9)$$

at the top and bottom electrode-film interface of the ferroelectric where the extrapolation length, λ , is taken as infinite. Periodic boundary conditions are used along the x -axis, i. e.,

$$P_3(z, x = 0) = P_3(z, x = L), P_1(z, x = 0) = P_1(z, x = L) \quad (10)$$

We apply Dirichlet boundary conditions to solve P in the thin film capacitors. At the dead layer-electrode interfaces, $-h/2-d$ and $h/2+d$ ($d=0$ corresponds to ideal electrodes), $\phi = 0$ correspond to total charge compensation at the film-electrode interface while periodic boundaries are adopted along x . Figure 1 shows the geometry adopted. Note that the entire ‘‘capacitor system’’ is neutral as the charges from ionized impurities, whose density is ρ , accumulate on the electrodes.

Equations of state (Eqns. 2a-2b) along with the equations of electrostatics in (Eqns. 7-8) using relations given in Eqns. 3-6 are solved simultaneously for P components employing a Gauss-Seidel iterative scheme subject to boundary conditions mentioned above in Eqns. 9 and 10. The simulations always start with small fluctuations of z and x components of P around zero that later on develop into the domain structure depending on dead layer and film thickness. We limit ourselves to 10000 iterations

converging to a difference of about 10^{-8} between consecutive iterative P solution steps when ferroelectricity exists. Owing to the compressive in-plane misfit in (001) BaTiO₃ on (001) SrTiO₃ (about 2.5 %), only P_3 is the spontaneous polarization that, in addition when depletion charge exists, also contain the built-in polarization, P_b . Thus, from here onwards the ferroelectric part of P_3 will be denoted as P_f and the built-in part as P_b . Note that when $\rho=0$, there is only one solution and it is $P_3=P_f$.

3. Results and Discussion

3.1 Room temperature domain structures when $d=0$ (Ideal electrodes)

We start discussing our results for three different film thicknesses, 12 nm, 16 and 20 nm with perfect film-electrode interfaces obtained at room temperature (RT). Structures with depletion charge at the max density limit considered in our work (2×10^{26} ionized impurities/m³) that are thinner than 10 nm thickness are nearly always found to exist in an imprinted single domain state and is not of interest here. The reason for this outcome is discussed in the proceeding paragraphs. The films without any depletion charge also exist in a homogeneous monodomain state and are not discussed here again for brevity. In general throughout this work, we chose to study two different depletion charge densities that reflect moderate-high and very high impurity densities reported for such structures. Depletion charge densities as high as 10^{25-27} ionized impurities/m³ were reported³¹ and we remain around these (5×10^{25} ionized impurities /m³ for the moderate-high limit and 2×10^{26} for the high limit) values in our simulations.

Figure 2 displays the domain structures that form in films of various thicknesses that have a fixed volumetric depletion charge density corresponding to 2×10^{26} ionized impurities/ m^3 . Upon finding that low densities of depletion charge yield only a unidirectional P_f in thin films, we focus on the densities that do trigger domains in thick structures (>10 nm). As a comparison for example, the 8 nm thick film with the aforementioned depletion charge density (2×10^{26} ionized impurities/ m^3) does not undergo a domain stabilization owing to the “insufficient extent of inhomogeneity”, meaning it is not thick enough for the built-in field to render a highly inhomogeneous structure. By inhomogeneous, we mean here the dependence of the local transition temperature on the built-in electric field at that location. Extremely high densities of depletion charge ($>10^{27}$ ionized impurities/ m^3) could perhaps stabilize domains in films with ideal electrodes but is out of the main scope of our study.

In Figure 2, we give the total polarization along with the ferroelectric polarization and the latter is obtained by subtracting P_b from P_3 for 12 nm, 16 nm and 20 nm films. The P_b is found by running our calculations above the Curie point as it is nearly temperature insensitive and is the only solution corresponding satisfying Eqns. 2, 7-8. At 2×10^{26} ionized impurities/ m^3 , a saw-tooth type domain pattern develops at RT whose period is a function of thickness. Relatively lower depletion charge densities ($<10^{26}$ ionized impurities/ m^3) do not tend to stabilize domains and result in a uniaxial P_f whose amplitude is less in one half of the film than in the other half concomitant with the internal field distribution. Therefore, the formation of domains in thicker films is due to the highly inhomogeneous nature of the built-in field renormalizing the linear term in P_3 in Eqn. 2a. Thus, the amplitude of the variation in the local transition temperature

naturally becomes more profound towards the film boundaries with increasing thickness for a given constant charge density. Hence thicker structures are forced to undergo domain stabilization to minimize the depolarizing fields emanating from the inhomogeneous depletion charge field. The domain period in such a high inhomogeneous system becomes a function of position, somewhat similar to what has been reported for discrete graded structures [42]. The situation described that applies to our analysis is also schematically depicted in Figure 3 for clarity.

Those results reveal that the domain structures forming due to the depletion charge induced fields in systems with ideal electrodes is quite different from what occurs when dead layers are present. For instance, in the latter, ferroelectric polarization amplitude attains a maximum in the middle section of the film while saw-tooth type domains have the maximum amplitude of the ferroelectric polarization wave near the electrode interfaces.

3.2. Room temperature domain structures when $d=1$ (Dead layers present)

In the presence of dead layers ($d=1$ unit cell) and depletion charge, a competition between the two formations, each of which is a source of inhomogeneity, takes place. A set of structures at RT for three different thicknesses and two depletion charge densities are provided in Figure 4. The left hand side gives the domain structure in the absence of depletion charge while the right hand side is when depletion charge is present. Subtracting the P_b at each site from P_3 , we again get the P_f as we did in the previous subsection. Amongst the analyzed structures, relatively moderate density of depletion

charge (5×10^{25} ionized impurities/m³ in this work) slightly alters the domain wall angles with respect to the film normal along with a period change as will be discussed next. A charge density of 2×10^{26} stabilizes the saw-tooth domain structure that has the prominent maxima in the P_f profile at the domain tips, similar to the case when $d=0$. Such a formation indicates that thick films with high depletion charge densities are under “weaker influence” of the dead layers. Another effective way to enable the comparison of the domain periods in films with and without depletion charge for a given thickness would be to plot and discuss the wave vector k of domains ($k=2\pi/\lambda$ where λ is domain period) as a function of thickness as we do in the proceeding paragraphs.

Before discussing the probable changes in domain period when depletion charges are present in thin films, we give the results for the domain wave vector, k , we obtained both in our simulations and using the approach presented in Ref. 43 to validate the trends of our simulations for charge-free films in Figure 5a. A summary of the approach in Ref. 43 in a modified form (See also Ref. 44) is given in the Appendix for convenience. Arising from the numerical nature of the simulation study and the finiteness of the system investigated (despite periodic boundary conditions along the film plane), we do not get a smooth and gradual change in the domain period hence in k . Still, there is an excellent agreement with the results obtained using the methodology in the Appendix. Note the approach in the Appendix adopted from Refs. 43 and 44 analyzes the phase transition point considering linear equation of state. We find that the domain period does not nearly change at all with further cooling upon the transition from the paraelectric to the multidomain FE state and transforms from a sinusoidal pattern to a square-like one, making it feasible to compare k values at and below the transition. In other words, even

when our simulation temperatures are not the same as the temperatures at which the k values were found using the approaches in Refs. 43 and 44, the k 's in both their study and our simulations are directly comparable.

To visualize the impact of depletion charge on the domain structures in films with dead layers, we now discuss behavior of the wave vector, k of the P_f wave plotted as a function of film thickness for ionized impurity densities of 5×10^{25} and 2×10^{26} /m³. Our results for films at RT without and with depletion charge are in Figure 5b. The presence of electrical domains in films with depletion charge have persisted for the entire thickness range of interest in our study. The depletion charge density was kept constant at 5×10^{25} ionized impurities/m³ for the sake of demonstration. Domain period for films thinner than 12 nm with 5×10^{25} ionized impurities/m³ is smaller than the charge-free film, while 2×10^{26} ionized impurities/m³ follows more or less the charge-free film but with slightly larger k values. The general trend of the increase in k values for films thinner than 12 nm in our work might be perceived as an indication that the depletion charge amplifies the depolarizing field for a given set of material parameters (domain wall energy, fixed dead layer thickness and dielectric constant and etc.). But this trend changes with increasing film thickness for the films having 5×10^{25} ionized impurities/m³ with respect to the charge-free case. Around 15 nm, a crossover occurs after which the thicker films with 5×10^{25} ionized impurities/m³ carrier density develop a coarser domain structure. Here, from the data of our simulations, we can see that the domain period is altered in a way the depolarizing field appears to be amplified, leading to a finer domain period hence a larger k . Still, we cannot arrive at general conclusions for the entire thickness regime we considered as thicker films (>16 nm) with moderate-high depletion charge density has a

distinctly different domain period. Despite the thought that any formation giving rise to or amplifying depolarizing fields will reduce the transition temperature, comparing the k values for a given thickness does not lead us to conclude so. To analyze the effect of depletion charge effects on the transition temperature, we carry out cooling runs in our simulations, extract and discuss the transition temperatures in the next section.

3.3. Phase transition temperatures

The paraelectric-ferroelectric transition temperatures for films with depletion charge is expected to be lowered in the presence of depletion charges, dead layers or when both coexist. Film thickness importantly comes into play in all of the cases above. Here we emphasize the situation when dead layers and depletion charges are both present but also run a case where the films at a thickness range of 3.2 nm to 24 nm have ideal electrodes for comparison. For reference, we first computed the transition temperature as a function of film thickness for a fixed dead layer thickness ($d=1$) and dielectric constant ($\epsilon_r=20$) and our results are in Figure 6a along with the results we obtained using the method prescribed in the Appendix. We find the transition temperatures by tracking $\langle |P_3| \rangle$ in our simulations. The transition temperatures computed from the numerical solution of Eqn. 16a in the Appendix has a very good match with the simulation results presented in this work, again confirming the validity of the prescribed method in Section 2. It must be borne in mind that the approach of Ref. 43 excludes gradient of P_3 (total polarization) along the thickness of the film, which we do include in our study. This can be the possible cause of the slight deviation between the two results at small thicknesses.

As expected, decreasing film thickness results in a reduction of the transition temperature with domain period subsequently becoming comparable or larger than the film thickness. Note that we do not go down to very low temperatures where ultrathin films (<3.2 nm in this work) might be in a single domain state upon transition from the paraelectric phase and that this takes place at quite low temperatures.

Computing the phase transition temperatures in films with dead layers but now with two different depletion charge densities, we note that films with a charge density of 5×10^{25} ionized impurities/m³ have nearly the same transition temperature compared to the charge free ones for a given thickness (See Figure 6b). Note that a homogeneous charge distribution does not lead to any net bias fields between the electrodes and no smearing of the transition exists, meaning the transition temperature is sharp. We then carried out the cooling runs for films having a depletion charge density of 2×10^{26} ionized impurities/m³ both in the presence and absence of dead layers to detect the transition. As mentioned previously, tracking $\langle |P_3| \rangle$ and comparing it with $\langle P_3 \rangle$ allows us to detect the phase transition if it is into a multidomain state. These films with 2×10^{26} ionized impurities/m³ and dead layers have a similar trend with the charge-free films at small thickness but then the transition temperature is significantly reduced for thicker films. Moreover, the transition temperatures in thicker films with and without dead layers are nearly the same. This scenario is certainly different for thinner films (<12 nm) and it is seen that the dead layers entirely dominate the transition characteristics (Compare the curves for the films having 2×10^{26} ionized impurities/m³ with and without dead layers in Figure 6b). This is solely due to the “degree of induced inhomogeneity” in the thicker films where the built-in electric field due to depletion charges induce a strong gradient of the transition

temperature via normalization of α_3^m in Eqn. 2, causing a larger amplitude variation of P_f , possibly overriding dead layer effects. Therefore, we provide quantitative evidence that the thicker films will be under a stronger influence of the depletion charge effects compared to thinner ones. One must remember here, however, that we discuss the case of rather high densities of depletion charge. For moderate-to-low densities ($<10^{25}$ ionized impurities/m³ in this work), the above discussion on transition temperatures merely converges to discussion of dead layer effects on the transition temperature as a function of film thickness.

4. Conclusions

We have analyzed the phase transition characteristics of ferroelectric thin films with and without depletion charge considering ideal electrodes and film-electrode interface with dead layers. Using the non-linear Landau-Ginzburg-Devonshire equation of state, simulations were carried out for films with different thicknesses at different temperatures to find the domain periodicities and transition temperatures as a function of depletion charge density at various thicknesses. The approach adopted from Ref. 43 and 44 has been used as a guide to check the validity of our simulation results. (001)BaTiO₃ grown on (001)SrTiO₃ with pseudomorphic electrodes was used as an example system. Films with high depletion charges split into saw-tooth type domains even when ideal electrodes are present. This happens when the film is above a critical thickness, below which a single domain, imprinted state is stabilized. Increase in film thickness naturally creates larger variations in the electric field, hence in local transition temperatures, due to

a constant density of depletion charge and a saw-tooth type domain structure is favored even in films with ideal electrodes to minimize the depolarizing fields. Presence of dead layers, when depletion charge densities are not very high ($<10^{26}$ ionized impurities/m³), determine the transition temperature both for thin (<10 nm) and thick films (>10 nm). At charge densities not very high, domain periods are slightly altered subsequent with tilted domain walls with respect to domain configurations in charge-free films. Although high charge densities in films with dead layers stabilize saw-tooth type domains regardless of the presence of the dead layers, the fact that very thin films (<10 nm) exist in a fine period multidomain state as opposed to what happens in films with ideal electrodes reveals the domination of the dead layer effects in thin films. While transition temperatures of ultrathin films having depletion charge are set by the dead layers, high depletion charge densities (2×10^{26} ionized impurities/m³ in this work) dominate over dead layer effects in thicker films. This can be judged by comparing the very similar results for these films with and without dead layers, i. e., the relatively thicker films with high depletion charge densities and dead layers have identical transition temperatures as those with same depletion charge density but ideal electrodes.

Acknowledgements

IBM has been partially supported by Turkish Academy of Sciences (TÜBA) through the GEBIP Program.

Appendix

The system analyzed in Ref. 43 is already given in Figure 1. The approach in Ref. 43 is based on finding the point of loss of stability of the paraelectric phase for a ferroelectric slab with dead layers. While the system in Ref. 43 is treated in one half of the film with dead layers as being vacuum and the film being very thick compared to the dead layers, this approach was generalized in Ref. 44 and we follow this general approach by full treatment of the film with high- k dead layers. Going back to the system in Figure 1, for a given dead layer thickness d (1 BaTiO₃ unit cell thick, ~ 0.4 nm, in this work) the boundary conditions of the system can be written as:

$$\mathbf{D}_F^z - \mathbf{D}_d^z = 0 @ z = \pm L/2 \quad (\text{A1})$$

where $D_F^z = \varepsilon_0 E_z^F + P$ and $D_d^z = \varepsilon_z^d \varepsilon_0 E_z^d$ are the dielectric displacements in the FE and dead layers respectively with ε_0 being the permittivity of vacuum in SI units, ε_z^d is the dielectric constant of the dead layer, P is ferroelectric polarization in the FE along the film thickness. The boundary conditions for the potential are as follows

$$\phi_F = \phi_d @ z = \pm L/2 \quad (\text{A2a})$$

$$\phi_d = 0 @ z = L/2 + d \quad (\text{A2b})$$

$$\phi_d = 0 @ z = -L/2 - d \quad (\text{A2c})$$

where $\phi_{F,d}$ are the potentials in the FE and the dead layer respectively. The electric fields in the layers can then be found from the gradient of the potentials. From Eqn. A1, one gets

$$-\varepsilon_0 \frac{d\phi_F}{dz} + P + \varepsilon_0 \varepsilon_z^p \frac{d\phi_d}{dz} = 0 @ z = L/2 \quad (\text{A3})$$

where L is the FE film thickness (See Figure 1). In the absence of free charges $divD = 0$ both in the FE and the dead layers. Writing these conditions in terms of the potential and polarization in the FE film, we get:

$$\frac{\partial^2 \phi_F}{\partial z^2} + \epsilon_{\perp} \frac{\partial^2 \phi_F}{\partial x^2} = \frac{1}{\epsilon_0} \frac{\partial P}{\partial z} \quad (\text{A4})$$

where ϵ_{\perp} is the dielectric constant of the FE along the plane of the film (Calculated as approximately 40 from the simulations and this value is used) and

$$\epsilon_0 \left(\epsilon_z^d \frac{\partial^2 \phi_d}{\partial z^2} + \epsilon_{\perp}^d \frac{\partial^2 \phi_d}{\partial x^2} \right) = 0 \quad (\text{A5})$$

for the dead layer. For convenience, it is assumed that the dead layer is isotropic and $\epsilon_z^d = \epsilon_{\perp}^d$ with ϵ_{\perp}^d being the dielectric constant of the dead layer along the film plane. The linear equation of state of the FE that is obtained by minimization of the Landau-Ginzburg free energy with its lowest order terms is:

$$AP - g \frac{\partial^2 P}{\partial x^2} = - \frac{\partial \phi_F}{\partial z} \quad (\text{A6})$$

where the gradient of P along z has been neglected as mentioned above, $A = (T - T_C) / \epsilon_0 C + M$ where T is temperature, T_C is the transition temperature in bulk form, C is the Curie constant, M represents any contribution of strain in the case of a FE on a substrate (See the modified coefficient of the lowest order term in P in the free energy in Ref. 36), g is the gradient energy coefficient. Note that the energy due to gradients along z is much less than the gradients of P along x , allowing one to safely neglect gradients along z . To solve the polarization and the potential using the differential equations above together with the equation of state in the FE, one can use the Fourier

transform to express the polarization and the potentials in the layers in terms of harmonics:

$$P = \sum_k P_k e^{ikx}, \quad \phi_F = \sum_k \phi_F^k e^{ikx}, \quad \phi_d = \sum_k \phi_d^k e^{ikx} \quad (\text{A7})$$

where P_k , ϕ_F^k and ϕ_d^k are the z -amplitudes of each harmonic in k . Inserting these Fourier transforms for a given k into Eqn.s A4, A5 and A6, we get:

$$\frac{d^2 \phi_F^k}{dz^2} + q^2 \phi_F^k = 0 \quad (\text{A8})$$

$$\frac{d^2 \phi_d^k}{dz^2} - k^2 \phi_d^k = 0 \quad (\text{A9})$$

where $q = (\varepsilon_\perp \varepsilon_0 k^2 |A + gk^2|)^{1/2}$. The solutions of Eqn.s A8 and A9 that satisfy the boundary conditions given in Eqn. A2 are:

$$\phi_F^k = A \cos qz + B \sin qz \quad (\text{A10})$$

$$\phi_d^k = C \sinh k(z - L - d) + D \cosh k(z - L) \quad (\text{A11})$$

where A , B , C and the D are the amplitudes in the general solution and

$$q = k \sqrt{\varepsilon_\perp \left(\frac{1}{\varepsilon_0 |A + gk^2|} - 1 \right)^{-1}} \quad (\text{A12})$$

Using the BCs given in Eqn.s A1 and A2c, we get two equations with two unknowns, B and C from Eqn.s A11 and A12:

$$B \left[q \cos \frac{qL}{2} + \frac{q}{\varepsilon_0 (A + gk^2)} \cos \frac{qL}{2} \right] - \varepsilon_z^d k C \cosh -\frac{kd}{2} = 0 \quad (\text{A13a})$$

$$B \sin \frac{qL}{2} - C \sinh -\frac{kd}{2} = 0 \quad (\text{A13b})$$

For a non-trivial solution to exist, the determinants of the coefficients in Eqn.s A14a and A14b has to be zero, giving us,

$$B \left[\sinh \frac{kd}{2} \left(q \cos \frac{qL}{2} + \frac{q}{\epsilon_0(A + gk^2)} \cos \frac{qL}{2} \right) + \epsilon_z^d k \cosh - \frac{kd}{2} \sin \frac{qL}{2} \right] = 0 \quad (\text{A14})$$

meaning that

$$\sinh \frac{kd}{2} \left(q \cos \frac{qL}{2} + \frac{q}{\epsilon_0(A + gk^2)} \cos \frac{qL}{2} \right) + \epsilon_z^d k \cosh - \frac{kd}{2} \sin \frac{qL}{2} = 0 \quad (\text{A15})$$

After some algebra on Eqn. A16, one gets

$$\tan \frac{qL}{2} = \frac{\sqrt{|\epsilon_k| \epsilon_\perp}}{\epsilon_z^d} \tanh \frac{kd}{2} \quad (\text{A16a})$$

where

$$|\epsilon_k| = \left(\frac{1}{\epsilon_0(A + gk^2)} + 1 \right) \quad (\text{A16b})$$

which was previously obtained by the authors of Ref. 43 through a similar route. Their approach is somewhat repeated here for tractability of results in our paper. We solve Eqn. A16a using a numerical approach and seek the k value that yields the highest transition temperature from the paraelectric state into the ferroelectric state for a given d (1 unit cell thick in this work). We do not carry out the calculations in the single domain state regime which correspond to thicknesses smaller than 3 nm and is outside the scope of our analysis. Also note that the described method is applied for the validation of the simulation results and do not reflect any depletion charge related effects, which are separately given only by the numerical simulation presented in this paper.

References

1. Triebwasser S., Phys. Rev. 1960; 118; 100.
2. Levanyuk A. P. and Sigov A. S., *Defects and Structural Phase Transitions*, Volume 6, in *Ferroelectricity and Related Phenomena*, edited by W. Taylor, Gordon and Breach Science Publishers, (1988).
3. Warren W. L., Dimos D., Pike G. E., Tuttle B. A., Raymond M. V., Ramesh R. and Evans J. T., Appl. Phys. Lett. 1995; 67; 866.
4. Shaw T. M., Troiler-McKinstry S., McIntyre P. C, Ann. Rev. Mat. Sci. 2000; 30; 263.
5. Ramesh R., Aggarwal S. and Auciello O., Mat. Sci. Eng. Rep. 2001; 32; 191.
6. Ganpule C. S., Roytburd A. L., Nagarajan V., Hill B. K., Ogale S. B., Williams E. D., Ramesh R. and Scott J. F., Phys. Rev. B 2002; 65; 014101.
7. Jin H. Z. and Zhu J., J. Appl. Phys. 2002; 92; 4594.
8. Chu M.-W., Szafraniak I., Scholz R., Harnagea C., Hesse D., Alexe M. and Gösele U., Nat. Mater. 2004; 3; 87.
9. Ren X., Nat. Mater. 2004; 3; 91.
10. Cockayne E. and Burton B. P., Phys. Rev. B 2004; 69; 144116.
11. Morozovska A. N. and Eliseev E. A., J. Phys: Cond. Mat. 2004; 16; 8937.
12. Balzar D., Ramakrishnan P. A. and Hermann A. M., Phys. Rev. B 2004; 70; 092103.
13. Alpay S. P., Misirlioglu I. B., Nagarajan V., Ramesh R., Appl. Phys. Lett. 2004; 85; 2044.
14. Zheng Y., Wang B. and Woo C. H., Appl. Phys. Lett. 2006; 88; 092903.

15. Batra I. P. and Silverman B. D., Sol. Stat. Comm. 1972; 11; 291.
16. Kretschmer R. and Binder K., Phys. Rev. B 1979; 20; 1065.
17. Bratkovsky A. M. and Levanyuk A. P., Phys. Rev. Lett. 2000; 84; 3177.
18. Junquero J. and Ghosez P., Nature 2003; 422; 506.
19. Wu Z. Q., Huang N. D., Liu Z. R., Wu J., Duan W. H., Gu B. L. and Zhang X. W., Phys. Rev. B 2004; 70; 104108.
20. Kim D. J., Jo J. Y., Kim Y. S., Chang Y. J., Lee J. S., Yoon J. G., Song T. K. and Noh T. W., Phys. Rev. Lett. 2005; 85; 237602.
21. Gerra G., Tagantsev A. K., Setter N. and Parlinski K., Phys. Rev. Lett. 2006; 96; 107603.
22. Ahluwalia R. and Srolovitz D. J., Phys. Rev. B 2007; 76; 174121.
23. Artemev A. and Roytburd A., Acta Mat. 2010; 58; 1004.
24. Wang Y., Niranjana M. K., Janicka K., Velez J. P., Zhuravlev M. Y., Jaswal S. S., and Tsymbal E. Y., Phys. Rev. B 2010; 82; 094114.
25. Zheng Y., Cai M. Q. and Woo C. H., Acta Mat. 2010; 58; 3050.
26. Cai M. Q., Zheng Y., Ma P.-W. and Woo C. H., J. Appl. Phys. 2011; 109; 024103..
27. Nathaniel N. G., Ahluwalia R., Su H. B., Boey F., Acta Mat. 2008; 57; 2047.
28. Dawber M., Rabe K. M., and Scott J. F., Rev. Mod. Phys. 2005; 77; 1083.
29. Bratkovsky A. M. and Levanyuk A. P., Phys. Rev. B. 2000; 61; 15042.
30. Matsuura H., New. J. Phys. 2000; 2; 8.1.
31. Xiao Y., Shenoy V. B. and Bhattacharya K., Phys. Rev. Lett. 2005; 95; 247603.
32. Okatan M. B., Mantese J. V. and Alpay S. P., Acta Mat. 2010; 58; 39.

33. Zhang Y., Li J. and Fang D., Phys. Rev. B 2010; 82; 064103.
34. Hong L., Soh A. K., Du Q.G. and Li J. Y., Phys. Rev. B 2008; 77; 094104.
35. Dawber M. and Scott J. F., Appl. Phys. Lett. 2000; 76; 1060.
36. Pintilie L. and Alexe M., J. Appl. Phys. 2005; 98; 124103.
37. Pintilie L., Boerasu I., Gomez M. J. M., Zhao T., Ramesh R. and Alexe M., J. Appl. Phys. 2005; 98; 124104.
38. Misirlioglu I. B., Okatan M. B. and Alpay S. P., J. Appl. Phys. 2010; 108; 034105.
39. Glinchuk M. D., Eliseev E. A. and Morozovska A. N., Ferroelectrics 2007; 354; 86.
40. Glinchuk M. D., Zaulychny B. Y. and Stephanovich V. A., Phys. Stat. Sol. 2006; 243; 542.
41. These coefficients are compiled from “Pertsev N. A., Zembilgotov A. G. and Tagantsev A. K., Phys. Rev. Lett. 1998; 80; 1988.”
42. Okatan M. B., Roytburd A. L., Mantese J. V. and Alpay S. P., J. Appl. Phys. 2009; 105; 114106.
43. Chensky E. V. and Tarasenko V. V., Sov. Phys. JETP 1982; 56; 618, Zh. Eksp. Teor. Fiz. 1982; 83; 1089.
44. Sidorkin A. S., *Domain Structure in Ferroelectrics and Related Materials*, Cambridge Int. Science Publishing, (2006).

Figure Captions

Figure 1. (Color Online) The schematic of the ferroelectric capacitor considered in this study.

Figure 2. (Color Online) The RT domain total polarization configurations of the (a) 12 nm, (b) 16 nm and (c) 20 nm thick films with 2×10^{26} ionized impurities/m³ and the extracted ferroelectric polarization given for (d) 12, (e) 16 and (f) 20 nm thick films on the right hand side. Scales are given to display the range of P_3 in C/m².

Figure 3. (Color Online) Schematic of the built-in field plotted as a function of position along the thickness of the ferroelectric film for a given homogeneous charge density (Right axis). The red curve indicates the variation of the Curie point along the thickness due to the built-in field.

Figure 4. (Color Online) Domain structures for (a) 12 nm, (b) 16 nm and (c) 20 nm thick films with dead layers. The right hand side of each colormap for a given thickness are the domain structures for $\rho = 5 \times 10^{25}$ (Upper colormap) and $\rho = 2 \times 10^{26}$ (Lower colormap). Scales are given to display the range of P_3 in C/m².

Figure 5. (Color Online) (a) Wave vector of the polarization along the film plane as a function of film thickness at the transition derived from solving Eqn. A16 for the point of loss of stability of the paraelectric phase summarized in the Appendix (red curve) and the wave vector we found in our simulations (blue squares) for $d=1$ unit cell. (b) Wave vector

of the polarization along the film plane as a function of thickness for films without charge (blue curve with diamonds), films having 5×10^{25} ionized impurities/ m^3 charge density (red curve with squares) and films having 2×10^{26} ionized impurities/ m^3 charge density (black curve with triangles) for $d=1$ unit cell. The curves in (b) passing through the data points are guides for the eyes.

Figure 6. (Color Online) (a) Phase transition temperatures in films with dead layers as a function of thickness when (a) No charge is present. The blue curve with diamonds are the results of our simulations and the red curve with squares are the results obtained by solving Eqn. A16 in the Appendix after Ref. 43. (b) Comparison of the results for charge-free (blue curve with diamonds), films having 5×10^{25} ionized impurities/ m^3 depletion charge (red curve with squares), films having 2×10^{26} ionized impurities/ m^3 depletion charge (black curve with triangles) and the green curve with triangles is the case for $d=0$ (no dead layer) and 2×10^{26} ionized impurities/ m^3 depletion charge given for comparison. Note that in (b) the red and blue curves have a strong overlap where the blue curve is just partially visible. The bulk transition temperature for (001)BaTiO₃ fully strained on (001)SrTiO₃ is 652°C.

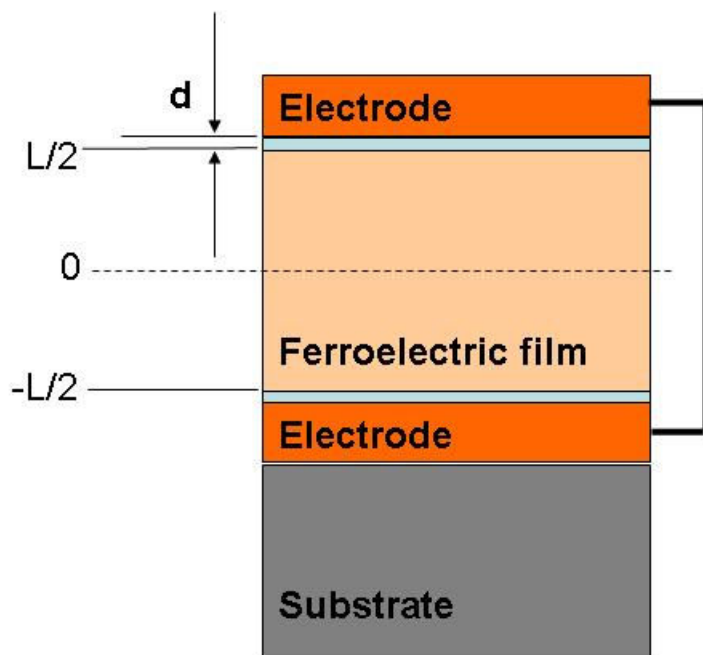


Figure 1.

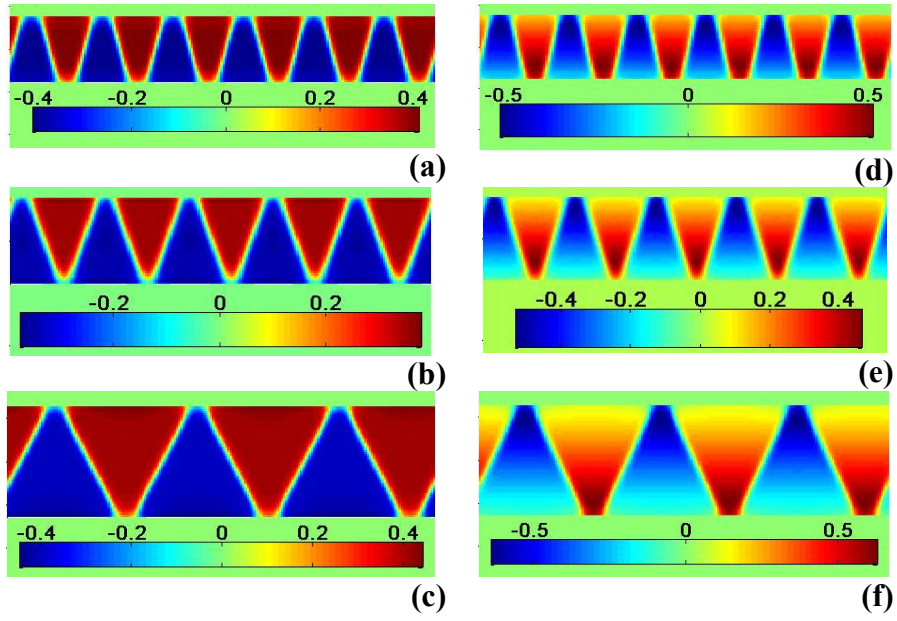


Figure 2.

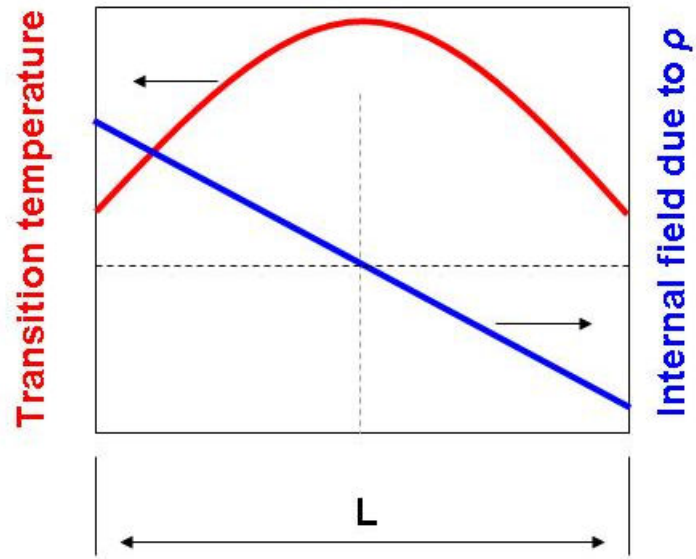


Figure 3.

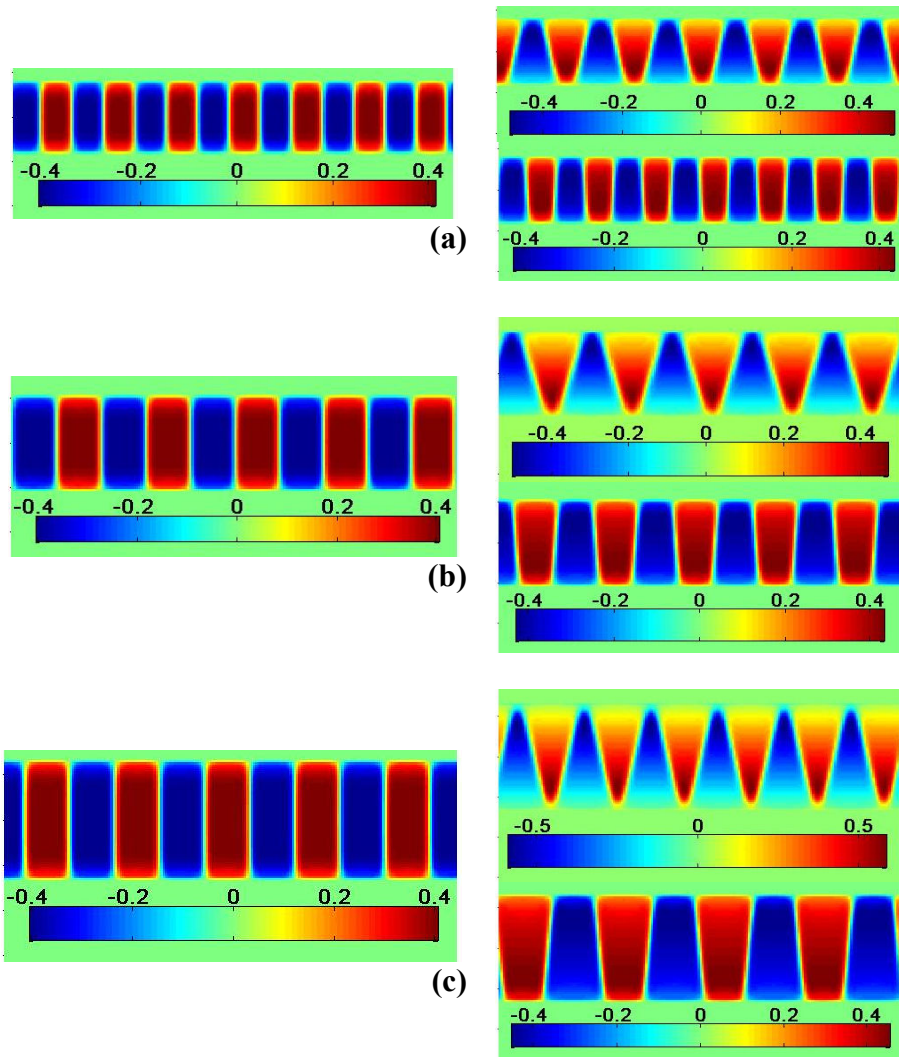


Figure 4.

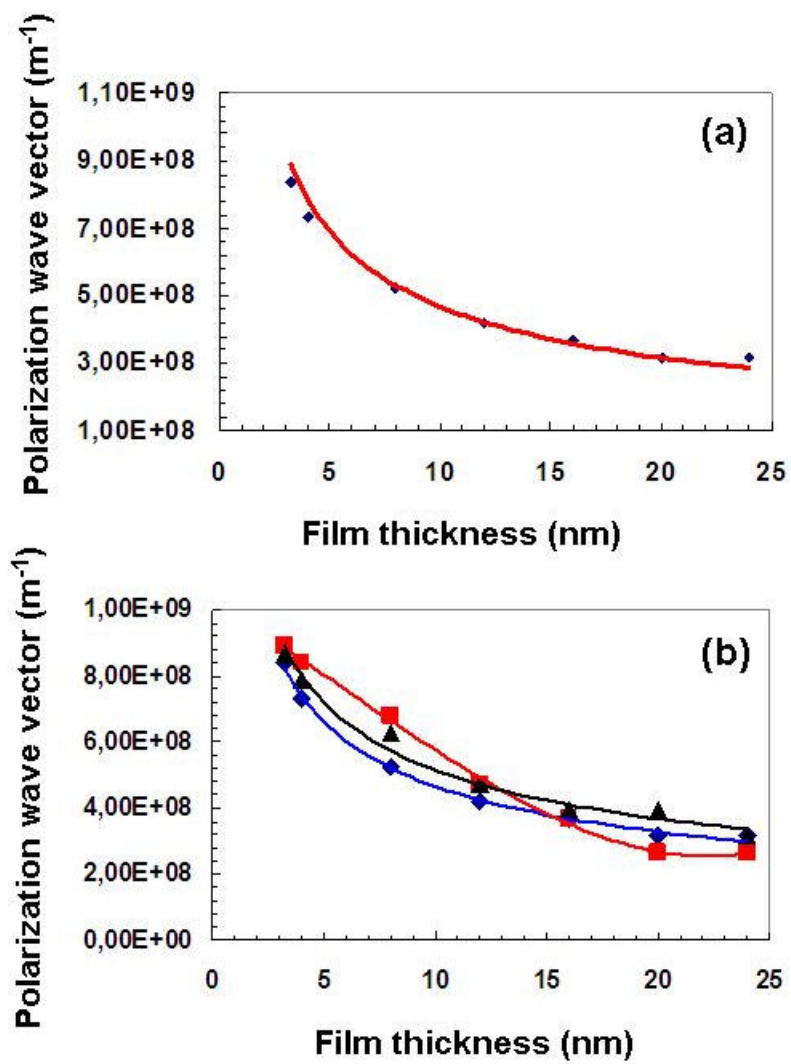


Figure 5.

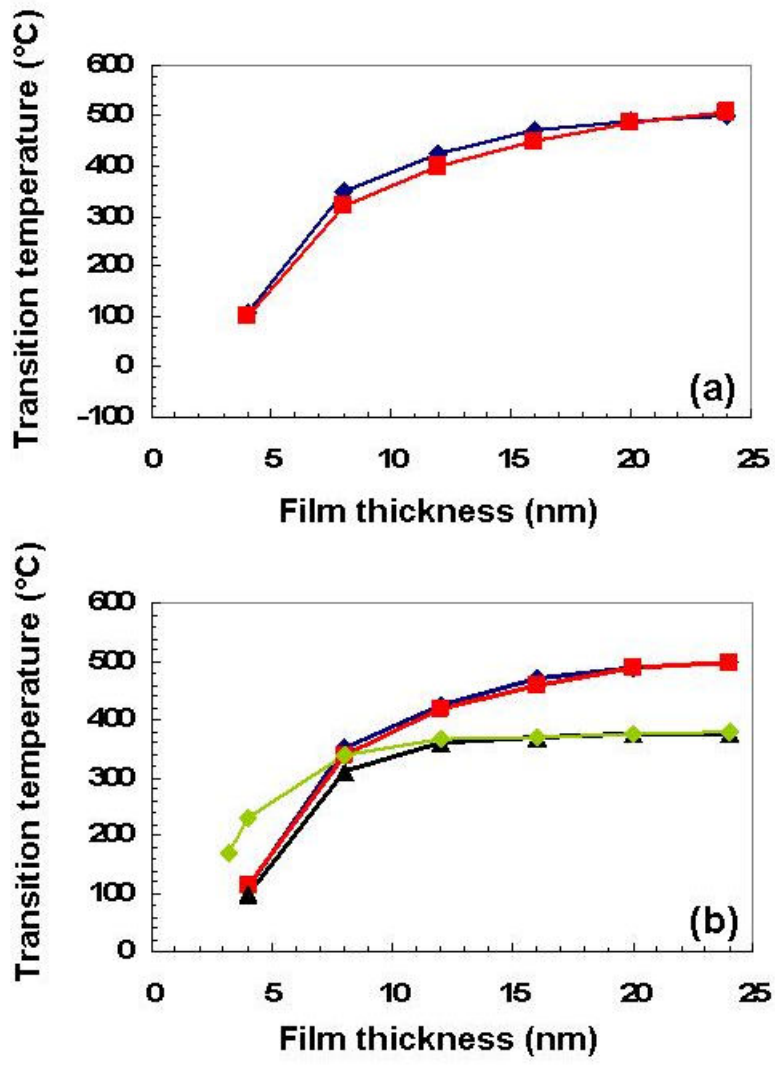


Figure 6.

